Seasonal Variation of Upper Tropospheric and Lower Stratospheric Equatorial Waves over the Tropical Pacific

CHRISTOPHER K. WIKLE*

Department of Geological and Atmospheric Sciences, Department of Statistics, Iowa State University, Ames, Iowa

ROLAND A. MADDEN

National Center for Atmospheric Research,+ Boulder, Colorado

TSING-CHANG CHEN

Department of Geological and Atmospheric Sciences, Iowa State University, Ames, Iowa

(Manuscript received 28 June 1996, in final form 8 January 1997)

ABSTRACT

Upper tropospheric and lower stratospheric wind data spanning 31 years from 1964 to 1994 were analyzed at rawinsonde stations in the central/western Pacific. Traditional spectral and cross-spectral analysis led to the conclusion that there is a significant signal with periods between 3 and 4.5 days, which the authors link with the dominant antisymmetric waves predicted by theory to have these periods, mixed Rossby–gravity waves, and equatorial Rossby waves. Then the authors applied the seasonally varying spectral analysis method developed by Madden to study the average seasonal variation of these waves. The seasonally varying analysis suggested that there are significant twice-yearly maxima in equatorial wave activity throughout the upper troposphere and lower stratosphere, with peaks occurring in late winter–spring and in late summer–fall. The twice-yearly signal was most prominent at the 70-hPa and 100-hPa levels. Similar and consistent results were also shown by an autoregressive cyclic spectral analysis. The cyclic spectral analysis suggested that the frequency characteristics of the v-wind wave power are different during the two maxima at some stations. In addition, the seasonally varying squared coherence between the u and v winds and the associated phase implied that there is horizontal momentum flux associated with these waves and that the sign of the flux is different during the two maxima. The differences in wave characteristics during the maxima periods may be related to different wave modes, seasonal variation of the basic zonal state, or possibly to different equatorial wave forcing mechanisms (i.e., convective versus lateral excitations).

1. Introduction

The foundation of the theory of equatorial waves was presented in the landmark paper of Matsuno (1966). Matsuno showed, using a simplified set of hydrodynamical equations, that equatorially confined wave solutions (among them the westward propagating mixed Rossby–gravity wave) were theoretically possible in tropical regions. Mixed Rossby–gravity waves (MRGWs) were first observed in rawinsonde data by Yanai and Maruyama (1966). Subsequently, numerous studies were conducted to identify the characteristics of MRGWs in both the troposphere and stratosphere (e.g., Maruyama and Yanai 1967; Maruyama 1967, 1969, 1979; Yanai et al. 1968; Yanai and Murakami 1970a,b; Nitta 1972). As summarized by Andrews et al. (1987), these studies have shown that MRGWs in the lower stratosphere generally have wavenumber-4 longitudinal scale with westward phase propagation and periods in the range of 3–5 days.

Theoretical (Lindzen and Matsuno 1968) and observational (e.g., Yanai and Hayashi 1969) studies suggest that lower stratospheric equatorial waves in the MRGW frequency range have a tropospheric origin. These waves are thought to originate from lateral forcing (Mak 1969), convective forcing (Hayashi 1970), or some combination of both mechanisms (e.g., Itoh and Ghil 1988; Goswami and Goswami 1991; Emanuel 1993). Observational and modeling evidence exists to support these hypotheses (e.g., Nitta 1970; Hayashi and Golder 1978; Zangvil and Yanai 1980,1981; Yanai and Lu 1983; Hendon and Liebmann 1991; Dunkerton and Baldwin 1995; Magaña and Yanai 1995).

*Current affiliation: NCAR/Geophysical Statistics Project, Boulder, Colorado.

+The National Center for Atmospheric Research is sponsored by the National Science Foundation.

Corresponding author address: Dr. Christopher K. Wikle, NCAR, P.O. Box 3000, Boulder, CO 80307-3000.
E-mail: wikle@ucar.edu

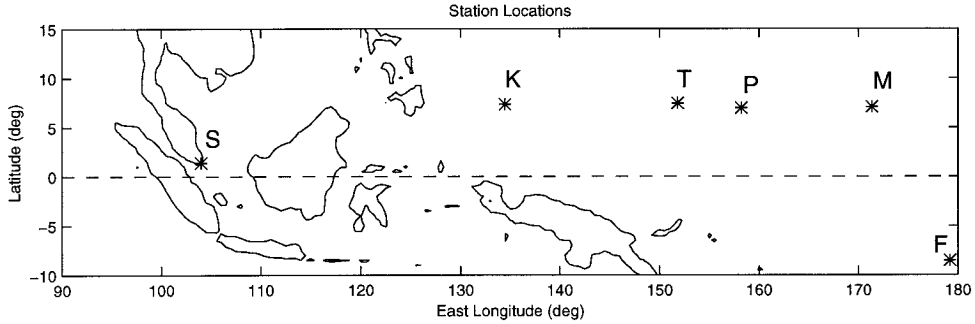

FIG. 1. Geographical locations of stations discussed in the analysis. S: Singapore, K: Koror, T = Truk, P = Ponape, M = Majuro, F = Funafuti.

Although there have been numerous studies on the spectral characteristics of equatorial waves and their potential forcing mechanisms, until recently little work has examined the seasonal variability of these waves. These recent studies have not shown a consistent seasonal structure for waves in the MRGW frequency range. For instance, observational studies have suggested peak wave activity in the lower stratosphere from midwinter to early summer, depending on geographical location (e.g., Dunkerton 1990, 1991, 1993; Maruyama 1991). For the equatorial upper troposphere, both modeling (Hayashi and Golder 1980) and observational (Dunkerton 1991) studies have suggested a primary peak of wave activity in the northern summer and a secondary peak in the northern winter. Observational studies of middle tropospheric waves have suggested peaks in the northern fall and winter (e.g., Hendon and Liebmann 1991; Dunkerton and Baldwin 1995).

Clearly, conclusions about the seasonal variability of the MRGWs have differed depending on pressure level, geographical location, and the atmospheric variable considered. In addition, we speculate that some of the differences in these studies may be a result of different analysis methods and data record lengths. Thus, the intent of this paper is to reexamine the average seasonality of upper-tropospheric and lower-stratospheric equatorial waves at several stations in the central and western Pacific using a relatively long data record (1964–94). Unlike previous studies, we use the seasonally varying spectral analysis (SVSA) method developed by Madden (1986) and a recently developed method, which we refer to as autoregressive cyclic spectral analysis (e.g., Sherman and White 1995). The results of these analyses suggest a twice-yearly peak in wave activity within the frequency range commonly associated with MRGWs in the upper troposphere and lower stratosphere. Furthermore, the seasonally varying cospectra suggest a variation in equatorial momentum flux associated with the waves in this frequency range, with the sign of the flux opposite for each wave activity maximum. The cyclic spectral analysis also suggests that the fundamental frequency of the wave activity varies with time at some stations. The data and methods are outlined in the next section. Section 3 presents the results of the analyses. A discussion of the results is given in section 4, and conclusions are presented in section 5.

2. Data and methods

a. Data

Time series of u and v components of the wind were extracted from rawinsonde archives at the National Center for Atmospheric Research (NCAR) at five tropical Pacific stations: Koror (7°20′N,134°29′E), Truk (7°27′N,151°50′E), Ponape (6°58′N, 158°13′E), Majuro (7°05′N,171°23′E), and Funafuti (8°32′S,179°13′E), for the years 1964–94. The Funafuti archive only contained reliable stratospheric data in the period from 1966 to 1971. The geographical locations of these stations are shown in Fig. 1. The periods 1966–72 and 1989–94 consisted primarily of twice daily observations (0000 and 1200 UTC), while the remaining years consisted of once-daily observations (0000 UTC). The 31-yr record allows us to examine the time-averaged seasonal behavior of equatorial waves. During quality control, suspect and missing data (5%–10% of the observations) were replaced by linear interpolation. This study primarily focuses on the 70-hPa level, although data from 150-, 100-, 50-, and 30-hPa levels are considered as well.

b. Methods

Spectral and cross-spectral analyses were performed using the smoothed periodogram method (Daniell 1946; e.g., Marple 1987, 153). A split-cosine bell taper (10% on each end) was applied to the data before the periodograms were calculated (e.g., Bloomfield 1976, p. 84), although the results were not sensitive to this taper.

To study the seasonal variation of equatorial waves over the 31-yr data record, the SVSA method developed by Madden (1986) and further outlined in Gutzler and Madden (1993) was used. In essence, one calculates the seasonal variation of the variance component associated with a time series after application of an a priori selected

bandpass filter. In our case, we apply a filter covering an equatorial wave frequency range to the u- and v-wind time series and then obtain the seasonally varying spectra, as well as the seasonally varying magnitude-squared coherence (MSC) and the associated phase.

In order to examine the seasonal variability of the full frequency spectrum, a cyclic spectral analysis was performed. Traditional spectral analysis techniques require an assumption of second-order stationarity (i.e., constant mean with autocorrelation depending only on time lag). This assumption clearly breaks down when the physical process under consideration has known cycles (e.g., solar influenced annual and semiannual cycles in atmospheric processes). In that case the mean and variance can be periodic. Traditionally, investigators remove these cycles, hoping that they then can satisfy the stationarity assumption. However, from a statistical perspective, it makes sense to use the information contained in the periodically correlated moments, rather than to remove it. Although the periodically correlated nature of atmospheric signals has been known for some time (e.g., Monin 1963; Jones 1964; Jones and Brelsford 1967; Hasselmann and Barnett 1981; Ortiz and Ruiz de Elvira 1985), there has not been much of an attempt to use this knowledge in spectral analysis. Recently there has been a surge of interest in these ideas in the engineering and time series literature, as well as the atmospheric science literature (e.g., Lund et al. 1995; Huang and North 1996). In particular, Huang and North (1996) demonstrated the utility of applying cyclic spectral analysis to cyclostationary atmospheric processes. They used a discrete Fourier transform (DFT) implementation of cyclic spectral analysis and applied it to a stochastic climate signal. Following the work of Sherman and White (1995), we implement an autoregressive (AR) cyclic spectral analysis, although we have extended the technique to the multiple time series case. As is the case with stationary model-based spectral techniques (e.g., maximum entropy and AR spectral analysis), the AR cyclic spectral formulation can give better spectral resolution with short time series than DFT approaches. A description of the methodology is included in appendix A.

3. Analysis

a. Identification of equatorial waves

It is difficult to identify completely and unambigously any phenomenon predicted by theory, particularly when faced with incomplete and noisy data. In this study, we are primarily interested in the frequency range traditionally associated with MRGWs. We will show variability in tropical lower stratospheric and upper tropospheric winds that is consistent in a number of ways with MRGWs. While we will use this variability as a marker for the presence of MRGWs, we cannot be absolutely certain that there is no other explanation.

Rossby–gravity waves in the lower stratosphere are thought to have a longitudinal scale of wavenumber 3–4 (e.g., Dunkerton 1991, 1993), with a period of 3–5 day and westward phase propagation at about 23 m s^{-1} (e.g., Andrews et al. 1987). Furthermore, the MRGW theoretical structure suggests that the waves are antisymmetric about the equator and that the v component of the wind should lead the u component by a quarter cycle ($\pi/2$) in the Northern Hemisphere (Matsuno 1966). Thus, we can attempt to identify the presence of MRGWs from the spectra of the u and v winds, as well as via the magnitude-squared coherence and associated phase between u and v. (MSC is not a useful indicator on the equator as the theoretical u component of the MRGW is zero there.)

As stated previously, the rawinsonde archive for stations used in our analysis includes twice-daily observations during two periods, 1966–72 and 2 October 1989–29 November 1994. We extracted twice-daily time series from both periods, each series containing 3770 observations (i.e., 1885 days in each of 2 Oct 1966–29 Nov 1971 and 2 Oct 1989–29 Nov 1994). The u and v spectra and cross-spectra were calculated for each data period, separately for each station, and the results were averaged [analogous to a Bartlett (1948) smoothing of the smoothed periodograms]. The power spectral estimates, MSC, and phase plots for Koror are shown in Fig. 2. Although the u-component power [$P(u)$] shown in Fig. 2a does not deviate significantly from a red noise spectrum for frequencies below 0.6 cycle/day (cpd), the v-component power [$P(v)$] shown in Fig. 2b shows a significant peak [relative to a 95% confidence level derived from an AR(1) red noise null hypothesis] in the frequency range between .22 and .38 cpd, corresponding to periods of 2.6–4.5 day. The MSC between the u and v time series [MSC(u, v)], shown in Fig. 2c, exhibits a distinct peak near .28 cpd (3.6 day). The region of significant MSC extends throughout much of the frequency domain. The MSC(u, v) phase plot in Fig. 2d shows that the v wind does indeed lead the u wind by a quarter of a cycle ($\pi/2$) in the MRGW frequency band. Note that the cross-spectral analysis for Funafuti (not shown) in the Southern Hemisphere exhibits similar MSC(u, v) results but with v lagging u by a quarter cycle, as expected by theory. The MSC(u, v) phase in the frequency range between .55 and .75 cpd shows that v lags u by a quarter cycle, but the associated MSC is relatively small.

To study the average propagation properties of wavelike disturbances, we perform a cross-spectral analysis between time series at different stations for the frequency band of interest. In particular, we consider the cross-spectral MSC analysis between the v components at each of the six possible combinations of four stations (Koror, Truk, Ponape, and Majuro), as shown in Fig. 3. The MSC (not shown) associated with the phases at frequencies shown in this plot are relatively large, although smaller with increasing station separation. If the

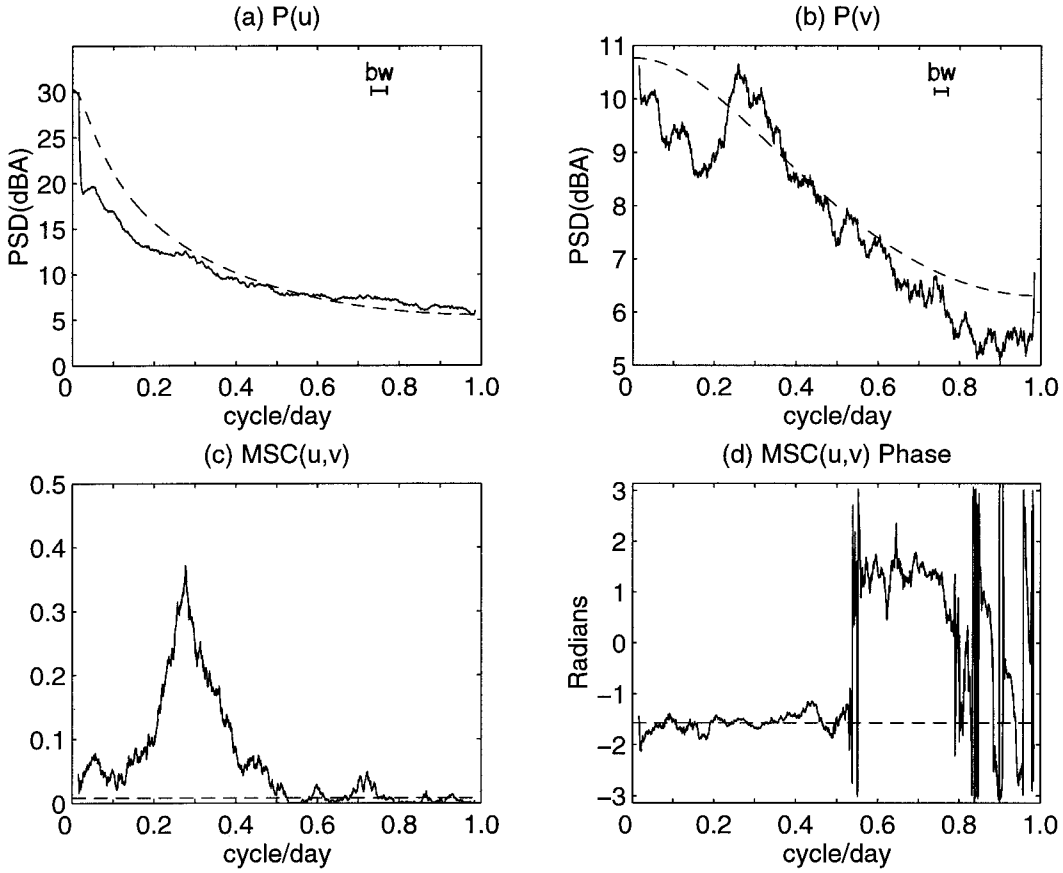

FIG. 2. Cross-spectral analysis of twice-daily 70-hPa u and v winds at Koror using a composite of two 1885-day periods, 2 Oct 1966–29 Nov 1971 and 2 Oct 1989–29 Nov 1994. Results were obtained using a smoothed periodogram method with smoothing bandwidth of .028 cycles per day (cpd). Dashed lines represent the 95% significance level of a red noise [i.e., AR(1)] null hypothesis. Solid lines represent (a) the power of the u wind in decibels [dBA: $dBA = 10 \log_{10} x$, where x is the power in (m s^{-1})^2·day], (b) v-wind power (dBA), (c) magnitude-squared coherence (MSC) between the u and v wind, and (d) the phase between u and v wind in radians; negative phase implies that the v wind leads the u wind. The dashed line in (d) does not represent the 95% significance level, but shows the theoretical $\pi/2$ phase difference between u and v.

phase is between zero and $-\pi$ then the v wind at the second station leads that at the first station. The reverse is true if the phase is positive. Thus, considering the longitudinal distribution of the stations, the phase propagation direction can be determined (e.g., Yanai et al. 1968). For instance, at .25 cpd the Truk–Majuro phase is negative, implying that the Majuro v wind leads that at Truk. Similarly, the Truk–Koror phase at the same frequency is positive, implying that the Truk v wind leads that at Koror. Since Koror is west of Truk, and Truk is west of Majuro, then the average phase propagation must be toward the west. Furthermore, the magnitudes of these phase differences are indicative of the horizontal scale of the wave. If the phase is plotted as a function of the difference in longitude (at a representative latitude) between the stations, then it is easily shown that the slope of the line is equal to the wavenumber. Based on Fig. 3, a linear regression of the longitude difference versus the MSC(v, v) phase gives an average wavenumber (slope) of 5.7 and 2.7 for frequency ranges of .15–.22 cpd (4.5–6.6 days) and .22–.33 cpd (3–4.5 days), respectively. Dividing the earth's circumference (at average station latitude 7.2°) by the wavenumber gives respective wavelengths of 7.0×10^3 and 14.8×10^3 km for the two frequency ranges. These wavelengths imply phase speeds of 16 and 43 m s^{-1}, respectively. Figure 3 then suggests that the equatorial wave phenomena with frequencies between .15 and .22 cpd have different characteristics than those in the frequency range .22–.33 cpd. In addition, there is a distinct phase transition at .33 cpd, suggesting that the predominant variability at frequencies above .33 cpd cannot be considered to be caused by westward propagating disturbances.

The wavenumber and phase speeds calculated here do not agree with the traditional wavenumber (3–4) and phase speed (-23 m s^{-1}) of equatorial stratospheric waves in the 3–5-day range. However, if we average

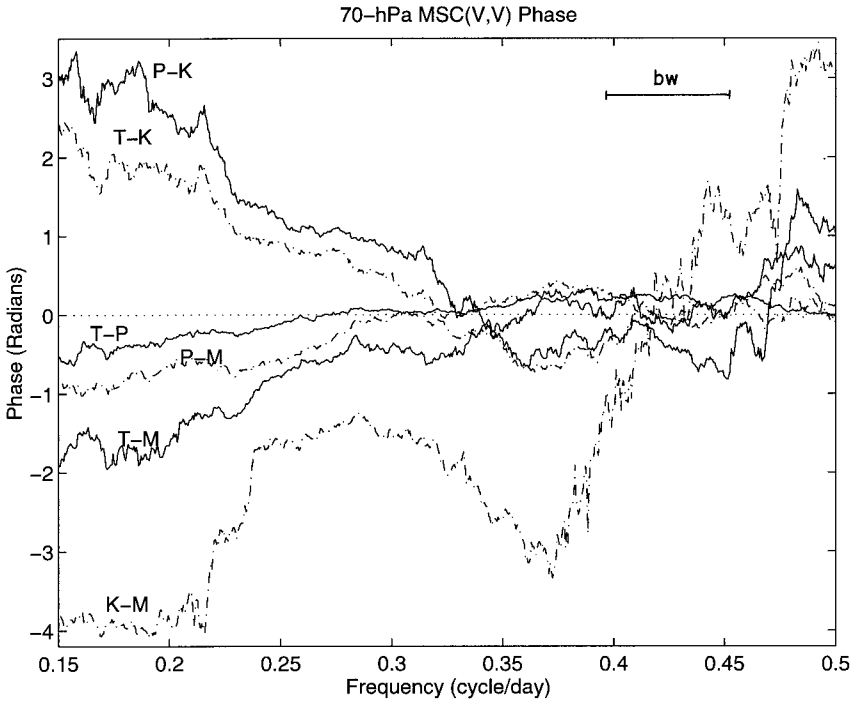

FIG. 3. MSC phase (rad) between the 70-hPa v wind at two stations using data and methods as for Fig. 2 except with a smoothing bandwidth of .056 cpd. Note that only a portion of the frequency domain is shown; the MSC (not shown) associated with the phase in this frequency range is relatively large, although decreasing with separation distance. Station symbols are: P(Ponape); K(Koror); T(Truk); M(Majuro), so that, for example, P–K represents the phase between v at Ponape and v and Koror.

our results over the 3–5 day range, then we get a wavenumber near 4 and a phase speed near -29 m s^{-1}, in much closer agreement with past estimates. These results suggest that it is probably not appropriate to consider a broad band (i.e., 3–5 day) when investigating the properties of equatorial waves.

It is certainly possible that the wave phenomena in these frequency ranges are not MRGWs as traditionally assumed, but a mixture of equatorial wave modes. Examination of equatorial wave theory (e.g., Matsuno 1966) suggests that the observed MSC(u, v) phase structure could also be indicative of the westward propagating equatorial Rossby modes ($n = 1$, 2 modes in the Matsuno theory). Without an adequate number of stations from which to examine the horizontal distribution of $P(v)$, it is difficult to distinguish between the Rossby modes and the the MRGW mode (i.e., n = 0 mode). However, as suggested by Yanai and Murakami (1970b), we can at least examine whether the predominant wave modes in a frequency range are odd ($n = 1$) or even ($n = 0$, 2) by examining whether they are symmetric or antisymmetric. This can be done if we have observations at roughly the same longitude on both sides of the equator. In our case, we can use Majuro and Funafuti, which are within 8° of longitude and are at roughly corresponding latitudes north and south of the equator, respectively. Then, if odd (i.e., symmetric) modes are the dominant wave mode, the cospectrum of zonal wind components between the stations should be positive and the cospectrum of meridional components should be negative. The opposite cospectrum relationships are true if the dominant modes are even (i.e., antisymmetric). Figure 4 shows the cospectra of the wind components between these stations at 70 hPa for the period 1966–71. On average, the results suggest dominant even wave modes in the .22–.33 and .36–.37 cpd frequency ranges, and dominant odd wave modes in the .06–.14, .34–.36, and .43–.48 cpd frequency ranges. The frequency range between .14 and .22 cpd does not show a consistent signal, suggesting that both odd and even modes contribute at these frequencies. Thus, the .15–.22 cpd range is likely to contain contributions from both equatorial Rossby and MRGW modes, which would complicate a seasonal analysis. Although we can be fairly certain that the $n = 1$ Rossby waves are not typically present in the .22–.33 range, we cannot distinguish between the $n = 2$ Rossby mode and the MRGW. However, given similar equivalent depths, theory suggests that the $n = 2$ mode should have a lower frequency than the MRGW.

Considering the region of significant $P(v)$ shown in Fig. 2b, along with the phase and cospectrum structure shown in Figs. 3 and 4, we will focus our seasonal analysis on the frequency band between .22 and .33 cpd. In light of the cospectrum results, we will then be con-

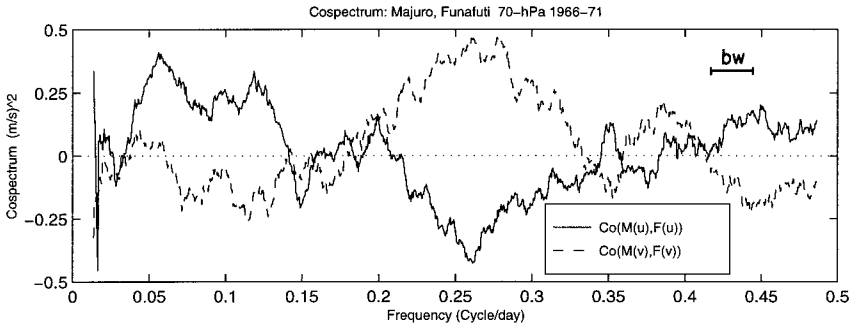

FIG. 4. Cospectrum (m s $^{-1}$)^2 of 70-hPa u-wind components (solid line) and v-wind components (dashed line) between Majuro and Funafuti during the period from 1966 to 1971. Results were obtained using a smoothed periodogram method with smoothing bandwidth of .028 cpd.

sidering the seasonal variation of the predominantly antisymmetric waves in this frequency band. It should be noted that not all of the power $P(v)$ in this frequency band is associated with such waves. In fact, the MSC analysis in Fig. 2c suggests that less than 40% of the variance in this band may be characterized as such.

b. Seasonal variation

The SVSA methodology was applied to the once-daily (0000 UTCZ) 70-hPa Koror time series over the 31 years from 1964 to 1994. As stated in the previous section, we will focus our seasonally varying (SV) analysis on the frequency band between .22 and .33 cpd. The sixth-order Butterworth bandpass filter (zero phase change) used to extract this frequency band from each time series for the SVSA analysis is shown in Fig. 5 (solid line). Since we are using once-daily observations, we must be concerned about possible aliasing of spectral power from frequencies higher than 0.5 cpd. The power

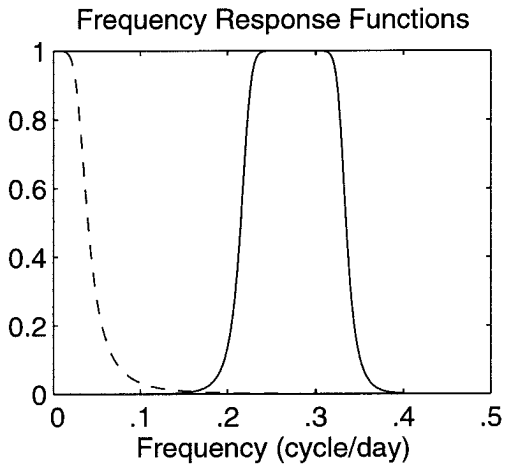

FIG. 5. Filter frequency response functions used in the seasonally varying spectral analysis. Solid line: Butterworth bandpass filter (order 6) with half-power points at .22 cpd (4.5 day) and .33 cpd (3 day). Dashed line: Butterworth low-pass filter (order 3) with half-power point at .033 cpd (30 days).

at these high frequencies, however, is minimal compared to that within the .22–.33 cpd frequency band (e.g., Fig. 2). Thus, we do not expect our results to be overly contaminated by aliased power.

The seasonal variance estimates of the filtered (.22–.33 cpd) u and v winds at Koror are shown in Fig. 6, along with the SV MSC(u, v) and phase. The SV estimates were smoothed by a low-pass Butterworth filter of order 3 and with half-power period of 30 days (Fig. 5, dashed line). The SV u wind in Fig. 6a has relative maxima in December–January and July. However, we do not focus on the u wind since $P(u)$ in the .22–.33 cpd frequency range is not significantly different from a red noise null hypothesis (Fig. 2a). The SV $P(v)$, shown in Fig. 6b, also exhibits twice-yearly maxima, but in mid-January–February and mid-August–October. The v-wind maxima are significant when compared to the 95th percentile of 500 identical SVSA analyses of simulated time series with cross-spectral structure similar to the Koror u and v winds but forced by Gaussian random noise (which should, on average, show no seasonal preference). These simulations were performed assuming a stochastic bivariate AR(4) process. The details of this simulation are included in appendix B.

It is important to reiterate that not all of the seasonally varying v-wind power in the frequency band we are considering can be associated with wave phenomena. Thus, it is beneficial to consider the MSC analysis as well. The SV MSC analysis (Fig. 6c) also shows a twice-yearly signal with maxima in mid-January–March and mid-June–September. These maxima are significant at the 95% level based on the SVSA simulations. The SV phase shown in Fig. 6d exhibits variability about the theoretical value ($-\pi/2$), with the first semiannual maximum corresponding to a more negative phase (v leads u by more than a quarter cycle), and the second maximum corresponding to a less negative phase (v leads u by less than a quarter cycle). Figure 7a shows the seasonally varying phase in detail. The variability in phase about the theoretical value ($-\pi/2$) suggests that there may be some dynamical differences between the

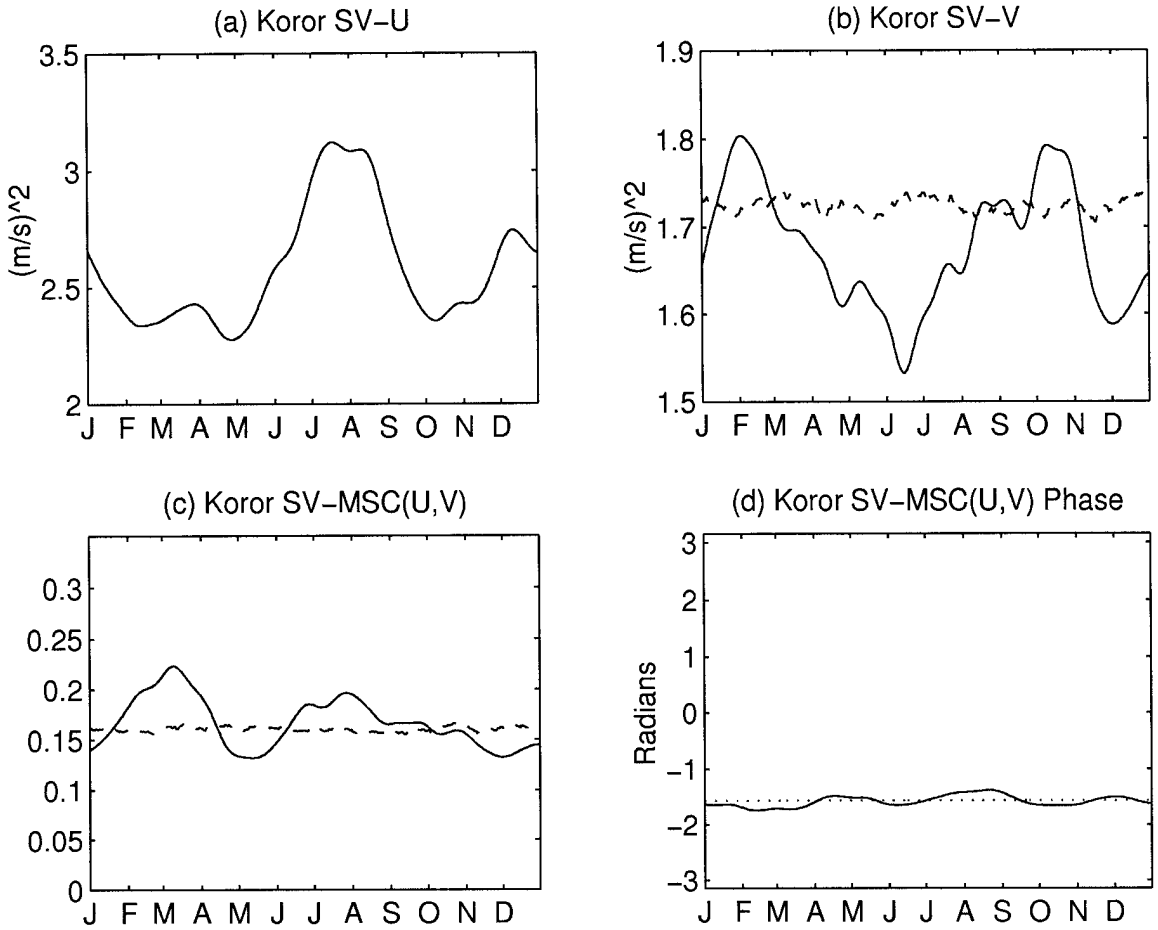

FIG. 6. Seasonally varying spectral analysis for 70-hPa Koror u and v winds with power in the range 3–4.5 day calculated with data from 1964 to 1994. Solid lines: (a) Seasonally varying (SV) u-wind variance (m s^{-1})^2, (b) SV v-wind variance (m s^{-1})^2, (c) MSC between u and v wind, (d) MSC phase (radians); negative phase implies that the v wind leads the u wind. Dashed lines: 95th-percentile significance level estimate obtained from 500 independent SV analyses using simulated data from a two-channel autoregressive model with similar spectral structure to the observed u and v winds (see appendix B). The 95th-percentile significance level for the SV u wind is near 3.5 (m s^{-1})^2, and is not shown.

waves occurring during late winter as compared to those during late summer.

From the definition of the SV MSC(u, v) phase [Eq. (8) in Madden 1986], a theoretical phase angle of $-\pi/2$ (i.e., v leads u by 90°) implies that the SV ''cospectrum'' [Eq. (4) in Madden 1986] must be zero (and is not zero when the phase deviates from this theoretical value). The SV ''cospectrum,'' however, is simply the SV covariance between the filtered u and v winds as a function of frequency and thus is a measure of horizontal eddy momentum flux. The SV cospectrum for Koror at 70 hPa is shown in Fig. 7b. Clearly, the cospectrum variability about zero follows the phase variability about $-\pi/2$. Thus, the phase difference between the SV MSC twice-yearly peaks (February and August) implies a cospectrum sign difference and, necessarily, a difference in horizontal momentum flux for the two semiannual maxima. It is possible, as described in Madden (1986) for MSC(u, v) phase differences associated with the 40–50-day oscillation, that these momentum flux differences could be due to seasonal variations in the upper-level northeast–southeast flow across the equator.

Although there are two maxima in both the SV v variance and SV MSC(u, v) shown in Figs. 6b and 6c, respectively, the maxima of these two measures occur at different times. Of course, all of the variability in the SV v wind need not be associated with the antisymmetric disturbances of interest here. In fact, the MSC(u, v) measure indicates that, at most, 23% of the SV variance in the v wind can be attributed to such waves. (Note that the difference between this result and the higher percentage suggested by Fig. 2 is due to the fact that the bandwidths of the spectral estimates shown in Fig. 2 are much smaller than those used in the SVSA.) In principle, the MSC and phase results between u and v should not be as sensitive to contamination from nonwave phenomena since the simultaneous analysis of multichannel data acts to filter noncoherent processes.

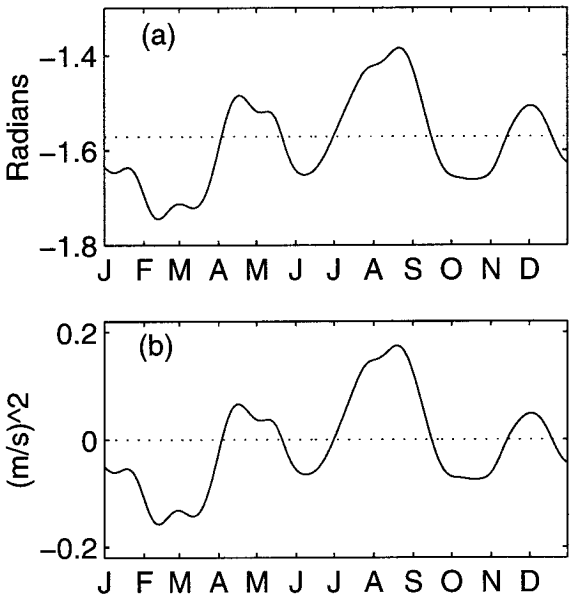

FIG. 7. Seasonally varying (a) MSC phase between u and v wind (radians), and (b) SV covariance (m s $^{-1}$)^2 at 70-hPa Koror calculated with data from 1964 to 1994.

This suggests that a useful marker of ''wave variance'' (i.e., wave ''activity'') could be obtained by multiplying the MSC by the v-wind variance. Such a marker would give a measure of the approximate variance associated with the wave modes in the frequency band of interest.

A plot of the seasonally varying $P(v) \times \text{MSC}(u, v)$ (i.e., the seasonally varying wave variance) for 70-hPa Koror, Truk, Ponape, and Majuro is shown in Figs. 8a–d, respectively. These plots show twice-yearly maxima at all locations, with the possible exception of Ponape. All stations exhibit late summer–early fall maxima. Koror and Truk show maxima in late winter–early spring, whereas Majuro (and perhaps Ponape) shows a winter maximum, as well. One possible explanation for the differences between the easternmost and westernmost stations is that the seasonality of the antisymmetric modes could be linked to the semiannual cycle in the global divergent circulation (e.g., through convection). In particular, Chen and Wu (1992) show that the semiannual cycle in the tropical divergent circulation has two centers, located at approximately 120°E and 160°W, which generally have opposite phase. Thus, it is possible that Majuro and Ponape are influenced by the eastern divergent center and Koror is influenced by the western center.

VERTICAL DISTRIBUTION

In light of the twice-yearly maxima in .22–.33 cpd v-wind wave variance at 70 hPa, it is useful to examine the seasonality of the wave variance throughout the upper troposphere and lower stratosphere. Figures 9a–d show contour plots of the SV v-wind wave variance

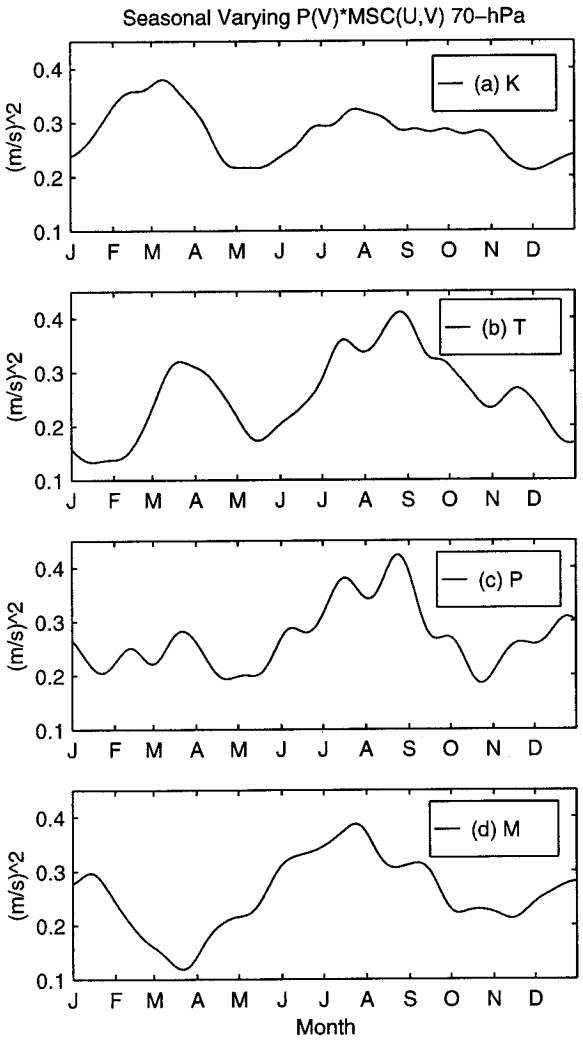

FIG. 8. Seasonally varying $P(v) \times \text{MSC}$ (u, v) in units (m s $^{-1}$)^2 at 70-hPa for (a) Koror, (b) Truk, (c) Ponape, and (d) Majuro, calculated with data from 1964 to 1994.

from 150 to 30 hPa for Koror, Truk, Ponape, and Majuro, respectively. These plots show that the v-wind wave variance maximizes near 100 hPa and is much smaller at 30 hPa, consistent with the likely increased dissipation of easterly waves in regions of stronger easterlies. The twice-yearly maxima are most evident at 100 and 70 hPa but are evident to a lesser extent at 150 and 50 hPa. The late winter–early spring maxima generally occur at the same time for each relevant level. However, these plots suggest that the late summer–early fall maxima may shift to lower levels with time.

We also consider the vertical distribution of the seasonally varying phase between the u and v winds. Figure 10 shows the SV MSC(u, v) phase at Koror for the 150-, 100-, 70-, 50-, and 30-hPa levels. There is a very interesting phase transition occurring in late spring, especially at 150 and 100 hPa. The phase at these levels suggests that the v wind leads the u wind by much more

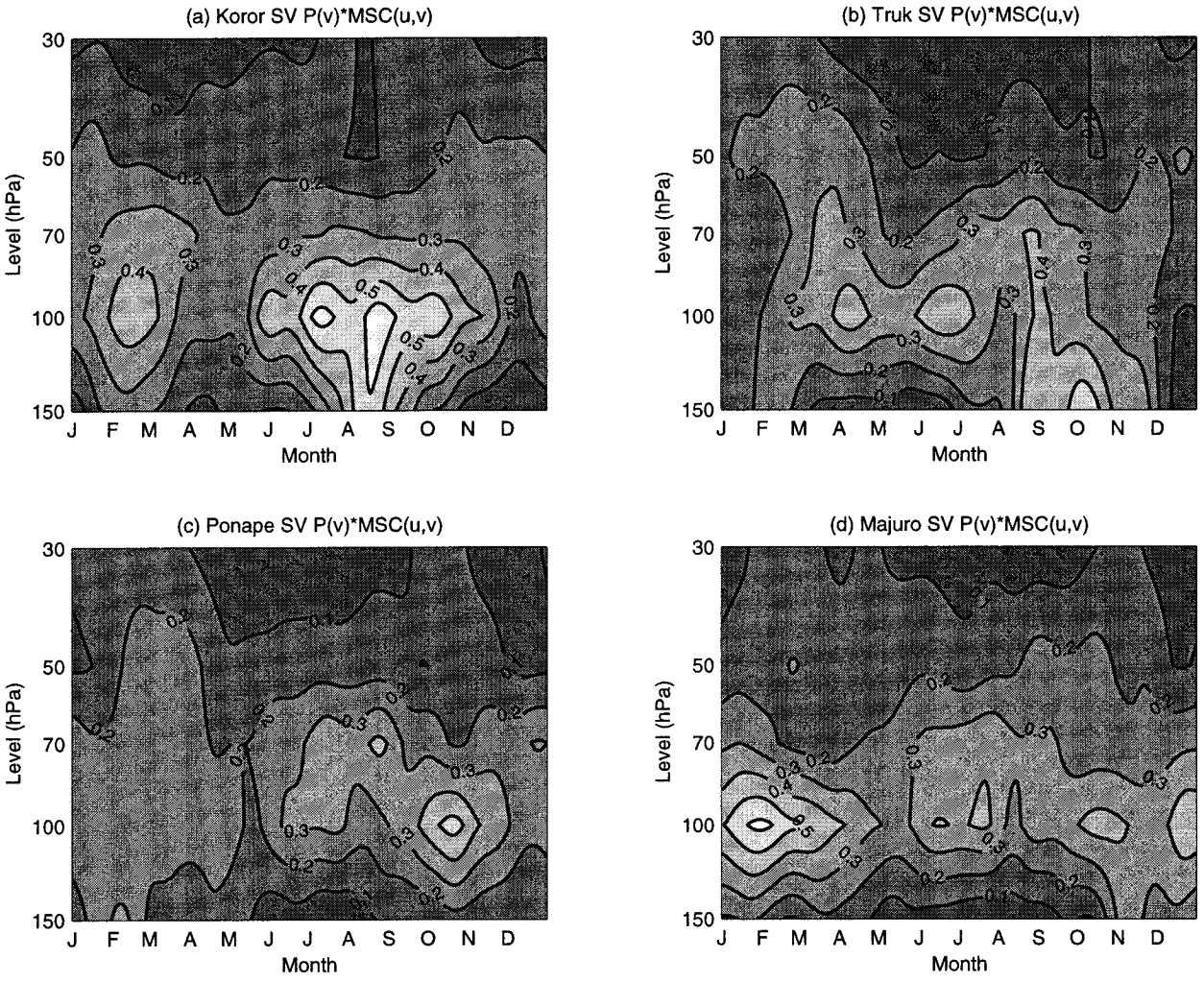

FIG. 9. Seasonally varying $P(v) \times \text{MSC}(u, v)$ in units $(\text{m s}^{-1})^2$ throughout the upper troposphere and lower stratosphere for (a) Koror, (b) Truk, (c) Ponape, and (d) Majuro, calculated with data from 1964 to 1994. Contour intervals are 0.1 $(\text{m s}^{-1})^2$.

than a quarter cycle in the winter and spring, and by much less than a quarter cycle in the summer and fall. As discussed above, this has implications with regard to the momentum flux associated with the waves and is possibly related to the seasonal variation of the upper-level flow from the summer to winter hemispheres (Madden 1986). However, the extreme phase differences in the upper troposphere call into question exactly what kind of phenomena are being captured by the seasonal analysis there. Results for the other stations (not shown) are qualitatively similar to those presented for Koror.

c. Cyclic spectral analysis

The seasonally varying analysis of the previous section suggested that there are significant twice-yearly peaks in .22–.33 cpd wave variance and that the characteristics of these waves may be different at different times of the year. We employ a cyclic spectral analysis as another test for the presence of twice-yearly maxima in equatorial wave activity and to examine the possibility of a seasonal shift in the frequency of the maxima. Such an analysis makes optimal use of the cyclostationary properties of the seasonal atmospheric data and allows us to examine the seasonal variability throughout the complete frequency range of the data. Our implementation is based on the autoregressive (AR) cyclic spectral techniques described in appendix A.

Figure 11 shows the $P(v) \times \text{MSC}(u, v)$ cyclic spectral estimates (i.e., wave activity) for Koror, Truk, Ponape, and Majuro. Although some guidance as to the most appropriate AR model order for the cyclic analysis can be obtained from a multivariate form of the Akaike AIC criterion (e.g., Marple 1987, 409), some ambiguity still remains as to the correct model order. Thus, we averaged cyclic spectral analysis results for model orders of 4 and 7. Furthermore, the cyclic spectra have been smoothed in time with a zero phase-shift Butterworth low-pass

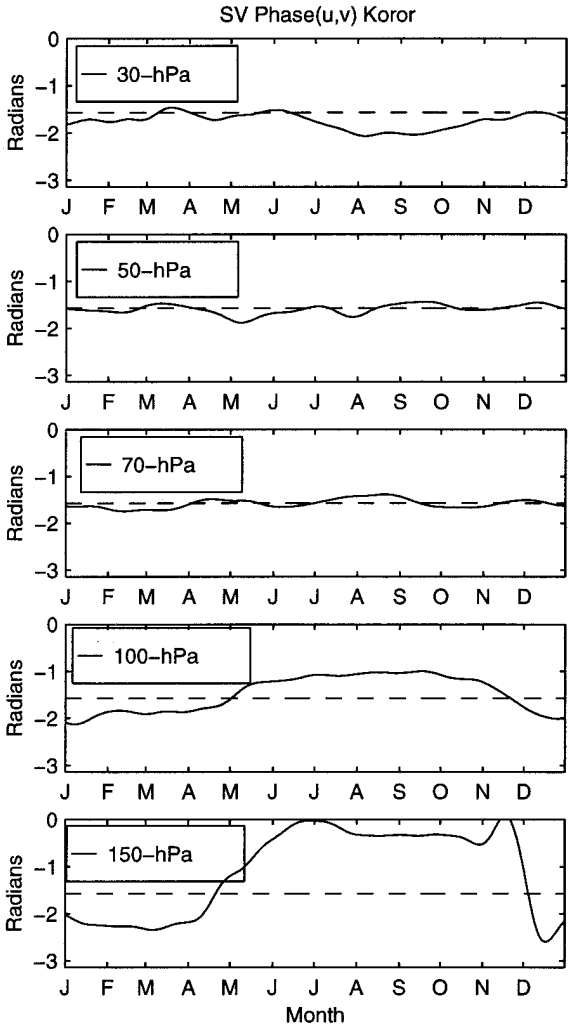

FIG. 10. Seasonally varying MSC phase (radians) between u and v wind at Koror for the 30-, 50-, 70-, 100-, and 150-hPa levels, calculated with data from 1964 to 1994.

filter of order 3 and with a half-power period of 60 days. Focusing on the .22–.33 cpd frequency band, we see that the twice-yearly maxima at each station are in good agreement with the average SVSA results shown in Fig. 8, with the exception that Fig. 11c shows a much clearer maximum in the spring at Ponape than the results shown in Fig. 8c. Perhaps more importantly, these plots suggest that there is a tendency for the maxima to propagate from higher frequencies to lower frequencies with time. This is particularly noticeable at Koror and Ponape in both the winter–spring and late summer–fall maxima but is not as obvious at Majuro and Truk in the late summer–fall maximum. These results suggest that the background zonal wind may be modifying the frequency characteristics of the equatorial waves. Figure 12 shows the average zonal wind for Koror, Truk, Ponape, and Majuro at 70 hPa. There is a strong annual cycle component to the zonal wind with maximum easterlies in the late summer and minimum easterlies in the late winter and early spring. Thus, the changes in frequency with time are consistent with the expected frequency change due to Doppler shifting (e.g., Andrews et al. 1987, 205). Furthermore, the minimum in wave activity occurring in the late spring–fall period corresponds to the period of rapidly increasing easterlies in the monthly averaged zonal wind, while the peaks correspond to the period of decreasing easterlies. This agrees with Maruyama's (1969) finding that equatorial waves in this frequency band are more prevalent when the absolute value of the zonal wind speed is decreasing in time.

We also note that at Koror and Ponape the late winter–spring maximum occurs at slightly lower frequencies than the late summer–fall maxima. The opposite is true at Majuro, and Truk does not show a large difference between the frequency range of the maxima. This provides further evidence that the waves in the first maximum have different characteristics than those in the second maximum.

4. Discussion

We have demonstrated by SVSA that there are most likely two seasonal periods of increased .22–.33 cpd equatorial wave activity in the western Pacific upper troposphere and lower stratosphere. These maxima were corroborated by autoregressive cyclic spectral analysis. Although the presence of the late winter–spring and late summer–fall peaks has been shown in numerical modeling (Hayashi and Golder 1980) and upper tropospheric observational studies (Dunkerton 1991), the latter peak in the lower stratosphere is at odds with recent observational studies (e.g., Maruyama 1991, hereafter M91; Dunkerton 1991, 1993, hereafter D91, D93). In addition, the late summer–fall maximum is intriguing since it is generally thought that westward propagating equatorial waves should be less likely in regions of relatively strong easterlies (i.e., Northern Hemisphere). We address these issues and discuss the implications of these findings in the following paragraphs.

First we address the apparent contradiction with recent observational results, which suggest only a late winter–spring maximum in lower stratospheric equatorial wave activity in this frequency range. That these earlier studies were unable to detect the late summer–fall maximum could be explained by such factors as the use of different wave markers, seasonal analysis techniques, data periods, analysis stations, and levels. For instance, both M91 and D91 focused more on $P(v)$ as a marker of wave activity, whereas we rely heavily on the coherence and quadrature relationship between u and v. In addition, both M91 and D91 used a sliding window of several month's length to examine seasonality. Although such a technique is adequate for studying the relationship of waves to the quasi-biennial oscillation and ENSO (which was the primary goal of these studies), the seasonal signal is ''smeared'' by the large

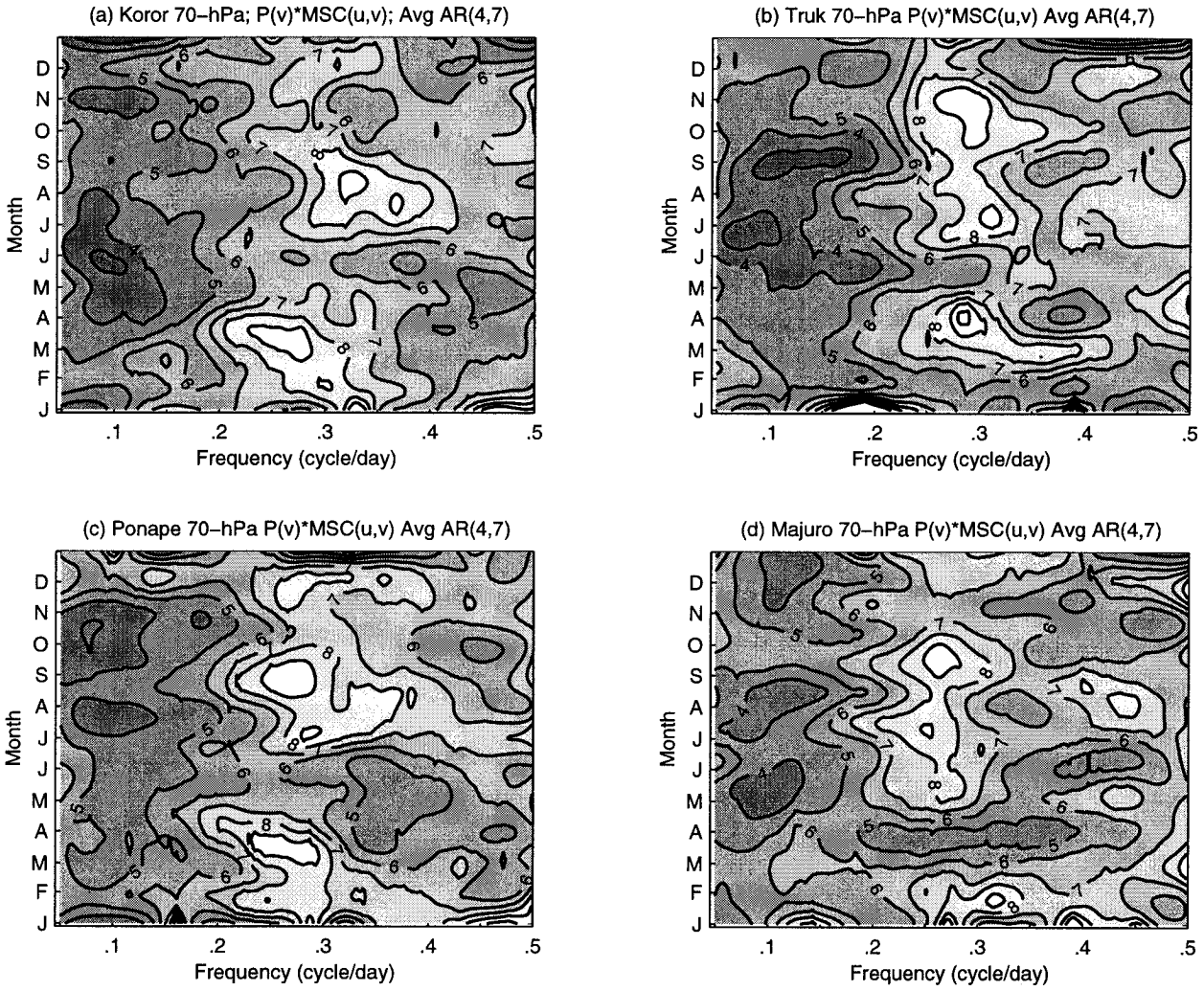

FIG. 11. Autoregressive cyclic spectral estimates of $P(v) \times \text{MSC}(u, v)$ in units of dBA (see Fig. 2) at 70 hPa for (a) Koror, (b) Truk, (c) Ponape, and (d) Majuro. The estimates were obtained by averaging the results of two separate cyclic spectral analyses performed on data from 1964 to 1994, assuming constant AR model orders of 4 and 7, respectively. The contour intervals are 1 dBA.

window. In addition, all of the previous studies have focused on the spectral characteristics of a relatively broad averaged spectral band, rather than the narrow spectral band used in our SVSA analysis and the examination of seasonal variation as a function of frequency, which we get from the cyclic spectral analysis. Furthermore, as shown by D91, the seasonal variation of equatorial waves in the 3–6-day range differs greatly depending on the geographical region of interest. Thus, given that M91 and much of D91 focus on wave activity over Singapore, it is not unexpected that the seasonality would be different than at our western and central Pacific stations (see Fig. 1). In fact, when using the SVSA technique with wind data from the 70-hPa level at Singapore, we did not find a late summer–fall peak in .22–.33 cpd wave activity (not shown). Finally, the pressure level of the data on which the analysis is performed could make a difference in the seasonal results, as evidenced from Fig. 9. Thus, although D93 examined seasonal variation of the quadrature spectrum of the two leading principal components of 50-hPa v-wind power derived from several Pacific stations (of which our stations are a subset), it is possible that the late summer–fall maximum does not propagate to 50 hPa (e.g., see Fig 9c,d), the weaker signal at that level cannot be detected by his analysis method, or that the combination of stations smears the signal.

We now consider the late summer–fall peak in .22–.33 cpd equatorial wave activity. It is well known from linear theory (e.g., Lindzen 1970, 1971; Andrews et al. 1987) that equatorial waves with intrinsically westward propagation require the mean zonal flow to be greater than the phase speed. Assuming that a late summer–fall forcing mechanism exists (e.g., convection), then fast equatorial waves could penetrate the easterly flow maximum that occurs during late summer in the lower strat-

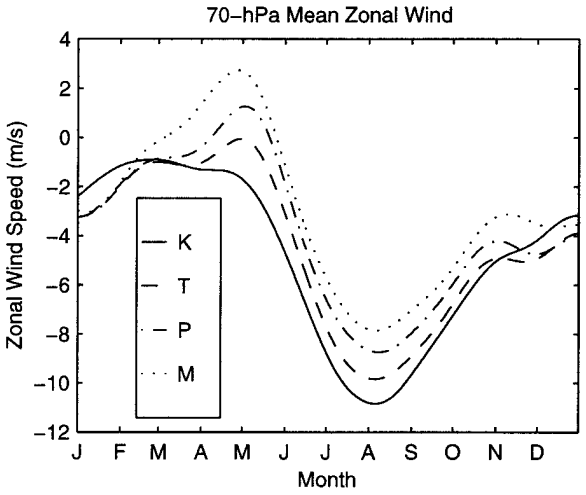

FIG. 12. Thirty-one year (1964–94) mean zonal wind (m s^{-1}) at 70 hPa for Koror (solid), Truk (dashed), Ponape (dash–dot), Majuro (dotted). The daily means have been smoothed with a Butterworth (order 3) low-pass filter with a half-power period of 60 days.

osphere. As we showed in section 3a, the equatorial waves in the higher frequency part of our range of interest have a relatively fast phase speed. These waves could easily penetrate the maximum average easterlies in the late summer (Fig. 12). Such waves would then be Doppler shifted to lower frequencies as the absolute value of the easterly regime decreased, in agreement with what is shown in Fig. 11.

Although this analysis cannot directly address the issue of equatorial wave forcing mechanisms, it is likely that the maxima in tropical convection occurring in the two solstice seasons are important. In that regard, the semiannual cycle in the global divergent circulation (and thus, the associated convection) could play a role (e.g., Chen and Wu 1992).

5. Conclusions

We analyzed 31 years of lower stratospheric wind data at several stations in the western/central Pacific. Traditional spectral and cross-spectral analysis led us to conclude that there is a significant signal in the range of 3–4.5 days and that the waves in this range are probably best characterized as mixed Rossby–gravity waves, but they could be characterized as antisymmetric equatorial Rossby waves (or some mixture of Rossby–gravity and Rossby modes). We then applied the seasonally varying spectral analysis (SVSA) method developed by Madden (1986) to study the average seasonal variation of these waves. The SVSA at 70 hPa for Koror suggested that there are significant twice-yearly maxima in v-wind power and the magnitude-squared coherence between the u and v wind. A more meaningful marker of wave activity was defined to be the v-wind power multiplied by the squared coherence between u and v. This measure showed maxima occurring in late winter–spring and in late summer–fall. These results were corroborated by an autoregressive cyclic spectral analysis.

Analysis of the wave activity throughout the upper troposphere and lower stratosphere exhibited a maximum near 100 hPa with a twice-yearly signal that is very clear at the 100- and 70-hPa levels. The twice-yearly signal was also present at other levels to a lesser extent, depending on location.

In addition, the SVSA squared coherence between the u and v winds and the associated phase implied that there may be horizontal momentum flux associated with these waves and that, locally, the sign of that flux is different during the two maxima. This effect seems to be magnified in the upper troposphere to the extent that it calls into question what wave phenomena are being characterized at these levels. The cyclic spectral analysis also suggested that the frequency of the v-wind wave activity is different during the two maxima. The differences in wave characteristics between the two maxima could be due to different wave modes (MRGW or equatorial Rossby wave), seasonal variation of the basic zonal state, or to different wave forcing mechanisms (i.e., convective versus lateral excitation mechanisms).

Additional efforts are required to further characterize the wave phenomena occurring in each maximum. Modeling studies could be used to explore the horizontal and vertical structure of the wave phenomena associated with the twice-yearly peaks as well as possible forcing mechanisms.

Acknowledgments. The research was sponsored in part by the U.S. Department of Energy, Office of Energy Research, Environmental Sciences Division, Office of Health and Environmental Research, under the first author's appointment to the Graduate Fellowships for Global Change administered by Oak Ridge Institute for Science and Education. Additional support for the first author was provided by the NCAR Geophysical Statistics Project, sponsored by the National Science Foundation under Grant DMS93-12686. Data and computer time were generously provided by NCAR during summer visits by the first author. Support was also provided by NSF Grant ATM-9416954. We wish to thank Peter Sherman for his discussions related to AR cyclic spectral analysis, Tim Dunkerton for his comments on an early draft, and two anonymous reviewers.

APPENDIX A

Autoregressive Cyclic Spectral Analysis

Daily and monthly atmospheric data typically show periodic structure due to the solar influenced annual and semiannual cycles. An excellent discussion of the analysis of periodically correlated atmospheric time series can be found in Lund et al. (1995). In addition, Huang and North (1996) provide a comprehensive discussion of cyclic spectral analysis related to atmospheric pro-

cesses. A more general and complete discussion of periodically correlated time series analysis from an engineering perspective can be found in Gardner (1994) and references therein. Our discussion of autoregressive cyclic spectral analysis loosely follows that found in Sherman and White (1995), who apply the technique to rotating machinery. However, we extend their approach to the multidimensional case.

A random process, Y_t, for $t \in 1, \cdots, n$ is defined as wide-sense cyclostationary (wsc) if both its mean $E[Y_t] \equiv \mu(t)$ and autocorrelation $E[(Y_s - \mu(s))(Y_t - \mu(t))] \equiv R(s, t)$ are periodic functions in t, with period d:

$$\mu(t) = \mu(t + kd) \tag{A1}$$

$$R(s, t) = R(s + kd, t + kd), \tag{A2}$$

for $k \in 0, \pm 1, \pm 2, \cdots$.

Now, assume that we have an m-dimensional process and, without loss of generality, assume that this process has zero mean. Define $\mathbf{y}_t$ to be an $m \times 1$ vector with each element corresponding to an element of a different time series at time t ($\mathbf{y}_t \equiv [Y_{1t}, \cdots, Y_{mt}]'$). We then assume that the process can be written in terms of a d-periodic vector autoregressive process,

$$\mathbf{y}_t - \sum_{j=1}^{p_t} \mathbf{A}_t(j)\mathbf{y}_{t-j} = \mathbf{e}_t, \tag{A3}$$

where $p_t = p_{t+d}$ is the AR model order for time t, $\mathbf{e}_t$ is an $m \times 1$ wsc white noise process such that $E[\mathbf{e}_t] = 0$, $E[\mathbf{e}_t\mathbf{e}_t'] \equiv \mathbf{\Sigma}_t = \mathbf{\Sigma}_{t+d}$, and $\mathbf{A}_t(j) = \mathbf{A}_{t+d}(j)$ are $m \times m$ cyclostationary AR parameter matrices.

By taking the multidimensional Z transform and expectation of both sides of (A3) (e.g., Marple 1987, 395), the $m \times m$ multidimensional cyclostationary power spectral density matrix can be written

$$\mathbf{P}(\omega, t) = [\mathbf{\Lambda}_{p_t}(t)\mathbf{\Omega}_{p_t}(\omega, t)^H]^{-1}\mathbf{\Sigma}_t[\mathbf{\Omega}_{p_t}(\omega, t)\mathbf{\Lambda}_{p_t}(t)^H]^{-1}, \tag{A4}$$

where

$$\mathbf{\Lambda}_{p_t} \equiv (\mathbf{I}_m \;\; \mathbf{A}_t(1) \cdots \mathbf{A}_t(p_t)) \tag{A5}$$

$$\mathbf{\Omega}_{p_t}(\omega, t) \equiv (\mathbf{I}_m \;\; \exp(i\omega)\mathbf{I}_m \cdots \exp(i\omega p_t)\mathbf{I}_m), \tag{A6}$$

and where $\mathbf{I}_m$ is an $m \times m$ identity matrix, ω is the spectral frequency, and the superscript $\{^H\}$ indicates a Hermitian matrix transpose.

In the $m = 2$ dimensional case, the cyclostationary power spectral densities for process 1 and 2 at frequency ω and time t are given by the (1, 1) and (2, 2) elements of the 2×2 matrix $\mathbf{P}(\omega, t)$, respectively. We denote these spectra as $P_{11}(\omega, t)$ and $P_{22}(\omega, t)$. In addition, the cyclostationary magnitude-squared coherence at frequency ω and time t is given by

$$\text{MSC}\ (\omega, t) \equiv |\Phi_{12}(\omega, t)|^2, \tag{A7}$$

where

$$\Phi_{12}(\omega, t) \equiv \frac{P_{12}(\omega, t)}{[P_{11}(\omega, t)P_{22}(\omega, t)]^{0.5}}, \tag{A8}$$

and where $P_{12}(\omega, t)$ is the off-diagonal element (1, 2) of the $\mathbf{P}(\omega, t)$ matrix. In addition, the corresponding MSC phase is given by

$$\text{PHS}(\omega, t) \equiv \tan^{-1}\left[\frac{\text{Im}\{\Phi_{12}(\omega, t)\}}{\text{Re}\{\Phi_{12}(\omega, t)\}}\right], \tag{A9}$$

where Im and Re refer to the imaginary and real parts.

a. Estimation

Pagano (1978) showed that a statistically consistent estimator for the autocorrelation of a one-dimensional wsc process is

$$\hat{R}(s, t) = N^{-1} \sum_{k=0}^{N-1} Y_{s+kd}Y_{t+kd}, \tag{A10}$$

where $N = n/d$, $Y_h = 0$ for $h \le 0$, and, without loss of generality, Y_t is taken to have zero mean. The corresponding estimate of $\mathbf{R}(s, t) \equiv E[\mathbf{y}_s\mathbf{y}_t^H]$ for the zero-mean m-dimensional case is given by

$$\hat{\mathbf{R}}(s, t) = N^{-1} \sum_{k=0}^{N-1} \mathbf{y}_{s+kd}\mathbf{y}_{t+kd}^H, \tag{A11}$$

where $N = n/d$ and $\mathbf{y}_h = 0$ for $h \le 0$.

We note that the Yule–Walker type equations corresponding to (A3) are

$$\mathbf{R}(t, t - \tau) = \sum_{k=1}^{p_t} \mathbf{A}_t(k)\mathbf{R}(t - k, t - \tau) + \delta_\tau\mathbf{\Sigma}_t), \tag{A12}$$

for $t = 1, \cdots d$; $\tau = 0, \cdots p_t$; and where $\delta_\tau = 1$ for $\tau = 0$ and zero otherwise.

By utilizing the consistent estimators given by (A11) in (A12), the Yule–Walker equations can be solved, giving consistent estimators of the parameters in the model (A3) (e.g., Pagano 1978). The Yule–Walker set can be solved via least squares or by a multidimensional version of Levinson's algorithm (e.g., Marple 1987, 400–402). Thus, with estimates of $\mathbf{\Sigma}_t$ and $\{\mathbf{A}_t(j), j = 1, \cdots, p_t\}$ for $t = 1, \cdots, d$, we can use (A5) and (A6) in (A4) to get the cyclic spectral estimates. In practice, for each t we pad the autoregressive parameter matrix $\mathbf{\Lambda}_{pt}$ with zero matrices in order to increase the resolution of the cyclic spectral estimates. Indeed, this is the advantage of using autoregressive (or maximum entropy) spectral methods when only short data records are available.

In practice, a choice must be made for the model orders at each time, p_t. A simple approach is to find the AR model order most appropriate for the time series [e.g., using a multidimensional form of Akaike's AIC criterion; see Marple (1987), 409] after having filtered for the frequency band of interest. In our case, we assume that $p_t = p$ for all t, where p is this "average" model order. Such an approach is somewhat naive, but

does provide a simple first approximation to the cyclic spectra. The optimal choice of AR model orders is a subject of current research (e.g., McLeod 1994).

We recognize the limitations inherent in the cyclic spectral approach. In particular, like any seasonal analysis, the cyclic spectral approach assumes that there is an underlying cycle that undergoes no variation in period. In fact, this may not be true (especially with daily data). It has been shown (e.g., Sherman and White 1995) that random variation in the cyclostationary period can seriously affect a seasonally varying analysis. Methods have been developed to track the underlying tonal frequency (e.g., using an extended Kalman filter). However, atmospheric scientists tend to be reluctant to deviate from the hypothesis of a rigid annual cycle since the year to year solar cycle variability is negligible. Furthermore, Wikle et al. (1995) showed that the 70-hPa annual cycle at a western Pacific station (Truk) has a very strong periodicity, nearly indistinguishable from a sinusoid. Thus, our assumption of a constant cyclostationary period is reasonable for the analyses performed in the current study.

APPENDIX B

Stochastic 2D AR Simulation

Consider a two-dimensional (i,e., two-channel) autoregressive process:

$$\mathbf{y}_t = \sum_{k=1}^{p} \mathbf{A}_k \mathbf{y}_{t-k} + \mathbf{e}_t, \tag{B1}$$

where p is the two-dimensional AR model order, $\mathbf{y}_t \equiv [y_{1t}, y_{2t}]'$, $\mathbf{A}_k$ is a 2×2 matrix of AR coefficients, and $\mathbf{e}_t \equiv [e_{1t}, e_{2t}]'$ is a zero-mean wide-sense stationary error process such that

$$E[\mathbf{e}_t \mathbf{e}_t'] = \begin{pmatrix} \sigma_1^2 & \sigma_{12} \\ \sigma_{21} & \sigma_2^2 \end{pmatrix}, \tag{B2}$$

where $\sigma_{12} = \sigma_{21}$.

We now present an algorithm that allows us to simulate from a two-dimensional (e.g., u and v wind) AR process of order p.

- Let $\mathbf{y}_t = [u_t, v_t]'$.
- Given $\mathbf{y}_t$ and a model order p [e.g., chosen via the multidimensional Akaike AIC criterion; Marple (1987), 409], estimate $\hat{\mathbf{A}}_k$, $\hat{\sigma}_1^2$, $\hat{\sigma}_2^2$, and $\hat{\sigma}_{12}$ by utilizing a method such as the multidimensional Levinson recursion algorithm (e.g., Marple (1987), 400–402).
- Simulate e_{1t} from $N(0, \hat{\sigma}_1^2)$ (i.e., a normal distribution with mean 0 and variance $\hat{\sigma}_1^2$).
- Simulate v_t from $N(0, 1)$ (i.e., a standard normal distribution).
- Let $e_{2t} = a^2\hat{\sigma}_1^2 + b^2$, where $a = \hat{\sigma}_{12}/\hat{\sigma}_1^2$ and $b = \hat{\sigma}_2^2 - \hat{\sigma}_{12}^2/\hat{\sigma}_1^2$ can be shown to give the appropriate two-dimensional AR error structure when $E(e_{1t}v_t) = 0$, for all t.
- Use the simulated e_{1t}, e_{2t}, and estimated $\hat{\mathbf{A}}_k$, $k = 1, \cdots, p$ in (B1) to generate as large a simulation of $\mathbf{y}_t$ as necessary, remembering to let the simulation ''burn in'' for a reasonable amount of time.
- Check the 2D spectra, cross-spectra, magnitude-squared coherence, and phase to verify that the simulated AR process is realistic in the portion of the frequency domain of interest. If not, the AR model order should be adjusted and the simulation repeated.

REFERENCES

Andrews, D. G., J. R. Holton, and C. B. Leovy, 1987: *Middle Atmospheric Dynamics.* Academic Press, 489 pp.

Bartlett, M. S., 1948: Smoothing periodograms from time series with continuous spectra. *Nature,* **161,** 686–687.

Bloomfield, P., 1976: *Fourier Analysis of Time Series.* John Wiley and Sons, 258 pp.

Chen, T.-C., and K. D. Wu, 1992: Semi-annual oscillation of the global divergent circulation. *Tellus,* **44A,** 357–365.

Daniell, P. J., 1946: On the theoretical specification and sampling properties of autocorrelated time-series. *J. Roy. Stat. Soc. Ser. B,* **8,** 88–90.

Dunkerton, T. J., 1990: Annual variation of deseasonalized mean flow acceleration in the equatorial lower stratosphere. *J. Meteor. Soc. Japan,* **68,** 499–508.

——, 1991: Intensity variation and coherence of 3–6-day equatorial waves. *Geophys. Res. Lett.,* **18,** 1469–1472.

——, 1993: Observation of 3–6-day meridional wind oscillations over the tropical Pacific, 1973–1992: Vertical structure and interannual variability. *J. Atmos. Sci.,* **50,** 3292–3307.

——, and M. P. Baldwin, 1995: Observation of 3–6-day meridional wind oscillations over the tropical Pacific, 1973–1992: Horizontal structure and propagation. *J. Atmos. Sci.,* **52,** 1585–1601.

Emanuel, K., 1993: The effect of convective response times on WISHE models. *J. Atmos. Sci.,* **50,** 1763–1775.

Gardner, W. A., 1994: An introduction to cyclostationary signals. *Cyclostationarity in Communications and Signal Processing,* W. A. Gardner, Ed., IEEE Press, 504 pp.

Goswami, P., and B. N. Goswami, 1991: Modification of n = 0 equatorial waves due to interaction between convection and dynamics. *J. Atmos. Sci.,* **48,** 2231–2244.

Gutzler, D. S., and R. A. Madden, 1993: Seasonal variations of the 40–50-day oscillation in atmospheric angular momentum. *J. Atmos. Sci.,* **50,** 850–860.

Hasselmann, K., and T. P. Barnett, 1981: Techniques of linear prediction for systems with periodic statistics. *J. Atmos. Sci.,* **38,** 2275–2283.

Hayashi, Y., 1970: A theory of large-scale equatorial waves generated by condensation heat and accelerating the zonal wind. *J. Meteor. Soc. Japan,* **48,** 140–160.

——, and D. G. Golder, 1978: The generation of equatorial transient planetary waves: Control experiments with a GFDL general circulation model. *J. Atmos. Sci.,* **35,** 2068–2082.

——, and ——, 1980: The seasonal variation of tropical transient planetary waves appearing in a GFDL general circulation model. *J. Atmos. Sci.,* **37,** 705–716.

Hendon, H. H., and B. Liebmann, 1991: The structure and annual variation of antisymmetric fluctuations of tropical convection and their association with Rossby-gravity waves. *J. Atmos. Sci.,* **48,** 2127–2140.

Huang, J.-P., and G. R. North, 1996: Cyclic spectral analysis of fluctuations in a GCM simulation. *J. Atmos. Sci.,* **53,** 370–379.

Itoh, H., and M. Ghil, 1988: The generation mechanism of mixed Rossby–gravity waves in the equatorial troposphere. *J. Atmos. Sci.,* **45,** 585–604.

Jones, R. H., 1964: Spectral analysis and linear prediction of meteorological time series. *J. Appl. Meteor.,* **3,** 45–52.
——, and W. M. Brelsford, 1967: Time series with periodic structure. *Biometrika,* **54,** 403–407.
Lindzen, R. S., 1970: Internal equatorial planetary-scale waves in shear flow. *J. Atmos. Sci.,* **27,** 394–407.
——, 1971: Equatorial planetary waves in shear: Part I. *J. Atmos. Sci.,* **28,** 609–622.
——, and T. Matsuno, 1968: On the nature of large-scale wave disturbances in the equatorial lower stratosphere. *J. Meteor. Soc. Japan,* **46,** 215–221.
Lund, R. B., H. L. Hurd, P. Bloomfield, and R. Smith, 1995: Climatological time series with periodic correlation. *J. Climate,* **8,** 2787–2809.
Madden, R. A., 1986: Seasonal variations of the 40–50 day oscillation in the tropics. *J. Atmos. Sci.,* **43,** 3138–3158.
Magaña, V., and M. Yanai, 1995: Mixed Rossby–gravity waves triggered by lateral forcing. *J. Atmos. Sci.,* **52,** 1473–1486.
Mak, M.-K., 1969: Laterally driven stochastic motions in the tropics. *J. Atmos. Sci.,* **26,** 41–64.
Marple, S. L., Jr., 1987: *Digital Spectral Analysis with Applications.* Prentice-Hall, 492 pp.
Maruyama, T., 1967: Large-scale disturbances in the equatorial lower stratosphere. *J. Meteor. Soc. Japan,* **45,** 391–407.
——, 1969: Long-term behavior of Kelvin waves and mixed Rossby–gravity waves. *J. Meteor. Soc. Japan,* **47,** 245–254.
——, 1979: Equatorial wave intensity over the Indian Ocean during the years 1968–1972. *J. Meteor. Soc. Japan,* **57,** 39–50.
——, 1991: Annual variations and QBO-synchronized variations of the equatorial wave intensity in the lower stratosphere at Singapore during 1961–1989. *J. Meteor. Soc. Japan,* **69,** 219–232.
——, and M. Yanai, 1967: Evidence of large-scale wave disturbances in the equatorial lower stratosphere. *J. Meteor. Soc. Japan,* **45,** 196–199.
Matsuno, T., 1966: Quasi-geostrophic motions in the equatorial area. *J. Meteor. Soc. Japan,* **41,** 25–42.
McLeod, A. I., 1994: Diagnostic checking of periodic autoregression models with application. *J. Time Ser. Anal.,* **15,** 221–233.
Monin, A. S., 1963: Stationary and periodic time series in the general circulation of the atmosphere. *Proceedings of the Symposium on Time Series Analysis,* M. Rosenblatt, Ed., Wiley, 144–151.
Nitta, T., 1970: On the role of transient eddies in the tropical troposphere. *J. Meteor. Soc. Japan,* **48,** 348–359.
——, 1972: Structure of wave disturbances over the Marshall Islands during the years of 1956 and 1958. *J. Meteor. Soc. Japan,* **50,** 85–102.
Ortiz, M. J., and A. Ruiz de Elvira, 1985: A cyclo-stationary model of sea surface temperatures in the Pacific Ocean. *Tellus,* **37A,** 14–23.
Pagano, M., 1978: On periodic and multiple autoregressions. *Ann. Statist.,* **6,** 1310–1317.
Sherman, P. J., and L. B. White, 1995: Improved periodic spectral analysis with application to diesel vibration data. *J. Acoust. Soc. Amer.,* **98,** 3285–3301.
Wikle, C. K., P. J. Sherman, and T.-C. Chen, 1995: Identifying periodic components in atmospheric data using a family of minimum variance spectral estimators. *J. Climate,* **8,** 2352–2363.
Yanai, M., and T. Maruyama, 1966: Stratospheric wave disturbances propagating over the equatorial Pacific. *J. Meteor. Soc. Japan,* **44,** 291–294.
——, and Y. Hayashi, 1969: Large-scale equatorial waves penetrating from the upper troposphere into the lower stratosphere. *J. Meteor. Soc. Japan,* **47,** 167–182.
——, and M. Murakami, 1970a: A further study of tropical wave disturbances by the use of spectrum analysis. *J. Meteor. Soc. Japan,* **48,** 185–197.
——, and ——, 1970b: Spectrum analysis of symmetric and antisymmetric equatorial waves. *J. Meteor. Soc. Japan,* **48,** 331–347.
——, and M.-M. Lu, 1983: Equatorially trapped waves at the 200-mb level and their association with meridional convergence of wave energy flux. *J. Atmos. Sci.,* **40,** 2785–2803.
——, T. Maruyama, T. Nitta, and Y. Hayashi, 1968: Power spectra of large-scale disturbances over the tropical Pacific. *J. Meteor. Soc. Japan,* **46,** 308–323.
Zangvil, A., and M. Yanai, 1980: Upper tropospheric waves in the tropics. Part I: Dynamical analysis in the wavenumber-frequency domain. *J. Atmos. Sci.,* **37,** 283–298.
——, and ——, 1981: Upper tropospheric waves in the tropics. Part II: Association with clouds in the wavenumber-frequency domain. *J. Atmos. Sci.,* **38,** 939–953.